Total Hadronic Cross-Section for Photon-Photon Interactions at LEP *

Frank Wäckerle[a]

[a]Fakultät für Physik, Albert-Ludwigs-Universität Freiburg, Germany

The total hadronic cross-section $\sigma_{\gamma\gamma}$ for the interaction of real photons, $\gamma\gamma \rightarrow$ hadrons, is extracted from a measurement of the cross-section of the process $e^+e^- \rightarrow e^+e^-\gamma^*\gamma^* \rightarrow (e^+e^- +$ hadrons) using a luminosity function for the photon flux and form factors for extrapolating to $Q^2 = 0$. The data was taken with the OPAL detector at LEP at e^+e^- centre-of-mass energies $\sqrt{s}_{ee} = 161$ GeV and 172 GeV. In the energy range $10 \leq W \leq 110$ GeV the total hadronic $\gamma\gamma$ cross-section $\sigma_{\gamma\gamma}$ is consistent with the Regge behaviour of the total cross-section observed in γp and hadron-hadron interactions.

1. Introduction

At high $\gamma\gamma$ centre-of-mass energies $W = \sqrt{s}_{\gamma\gamma}$ the total cross-section for the production of hadrons in the interaction of two real photons is expected to be dominated by interactions where the photon has fluctuated into an hadronic state. Measuring the $\sqrt{s}_{\gamma\gamma}$ dependence of the total hadronic $\gamma\gamma$ cross-section $\sigma_{\gamma\gamma}$ should therefore improve our understanding of the hadronic nature of the photon and the universal high energy behaviour of total hadronic cross-sections.

Before LEP the total hadronic $\gamma\gamma$ cross-section has only been measured for $\gamma\gamma$ centre-of-mass energies W below 10 GeV by PLUTO [1], TPC/2γ [2] and the MD1 experiment [3] where the high energy rise of the total cross-section could not have been observed. Using LEP data taken at e^+e^- centre-of-mass energies $\sqrt{s}_{ee} = 130 - 161$ GeV, L3 [4] has demonstrated that the total hadronic $\gamma\gamma$ cross-section in the range $5 \leq W \leq 75$ GeV is consistent with the universal Regge behaviour of total cross-sections. We present a measurement of the total hadronic $\gamma\gamma$ cross-section in the range $10 < W < 110$ GeV using OPAL data taken at $\sqrt{s}_{ee} = 161$ GeV and 172 GeV.

2. Kinematics

The kinematics of the process $e^+e^- \rightarrow (e^+e^- +$ hadrons) at a given $\sqrt{s}_{ee}$ can be described by the negative square of the four-momentum transfers, $Q_i^2 = -q_i^2$, carried by the two $(i = 1, 2)$ incoming photons and by the square of the invariant mass of the hadronic final state, $W^2 = s_{\gamma\gamma} = (q_1 + q_2)^2$ [5]. Events with detected scattered electrons (single-tagged or double-tagged events) are excluded from the analysis. This anti-tagging condition defines an effective upper limit Q_{max}^2 on the values of Q_i^2 for both photons. This condition is met when the scattering angle θ' of the electron is less than the angle $\theta_{max} = 32$ mrad between the beam axis and the inner edge of the acceptance of the detector or if the energy of the scattered electron is smaller than the minimum energy of 35 GeV required for the tagged electron.

3. Monte Carlo simulation

The leading order (LO) QCD Monte Carlo generators PYTHIA 5.722 [6] and PHOJET 1.05c [7] are used to simulate photon-photon interactions. PYTHIA is based on a model by Schuler and Sjöstrand [8] and PHOJET has been developed by Engel based on the Dual Parton model (DPM) [9]. The SaS-1D parametrisation of the parton distribution functions [10] is used in PYTHIA and the leading order GRV parametrisation [11] in PHOJET. The fragmentation and decay of the parton final state is handled in both generators by the routines of JETSET 7.408 [6].

4. Event selection

Two-photon events are selected by requiring that the visible invariant hadronic mass, W_{ECAL}, measured in the electromagnetic calorimeter (ECAL), has to be greater than 3 GeV. At least 3 tracks must have been found in the event and the sum of all energy deposits in the ECAL and the hadronic calorimeter (HCAL) has to be less than 45 GeV. The missing transverse energy of the event measured in the ECAL and the forward calorimeters (FD) has to be less than 5 GeV. No track in the event has a momentum greater than 30 GeV/c. Finally, to remove events with scattered electrons in the FD or the silicon tungsten calorimeter (SW), the energy measured in the FD has to be less than 50 GeV and the energy measured in the SW less than 35 GeV (anti-tagging condition).

Additional cuts are applied to reject beam-gas and beam-wall background. On average the trigger efficiency for the lowest W range, $10 < W < 30$ GeV, is greater than 97% and it approaches 100% for larger values of W.

We use data corresponding to an integrated luminosity of 9.9 pb^{-1} at $\sqrt{s}_{ee} = 161$ GeV and 10.0 pb^{-1} at $\sqrt{s}_{ee} = 172$ GeV. After applying all preselection cuts 55169 events remain. From the Monte Carlo (MC) it is estimated that after all cuts about 4% of all remaining events are $e\gamma$ processes with $Q^2 > 1$ GeV^2. The background from other processes apart from beam-gas and beam-wall interactions amounts to less than 1%.

5. W reconstruction

For measuring the total hadronic $\gamma\gamma$ cross-section $\sigma_{\gamma\gamma}$ the value of W must be reconstructed from the hadronic final state. After the event selection a matching algorithm is applied in order to avoid double counting of particle momenta. The matching algorithm uses all the information of the ECAL, the HCAL, the FD and the SW calorimeters, as well as the tracking system. The four-momenta of the detected particles are used to calculate the visible invariant mass W_{vis}.

A cut $W_{vis} > 6$ GeV is applied to all preselected events. The W_{vis} distribution $\mathrm{d}N/\mathrm{d}W_{vis}$

measured at 172 GeV is shown in Fig. 1 where N is the number of selected events. They are well described by the MC simulations which have been normalized to the number of data events.
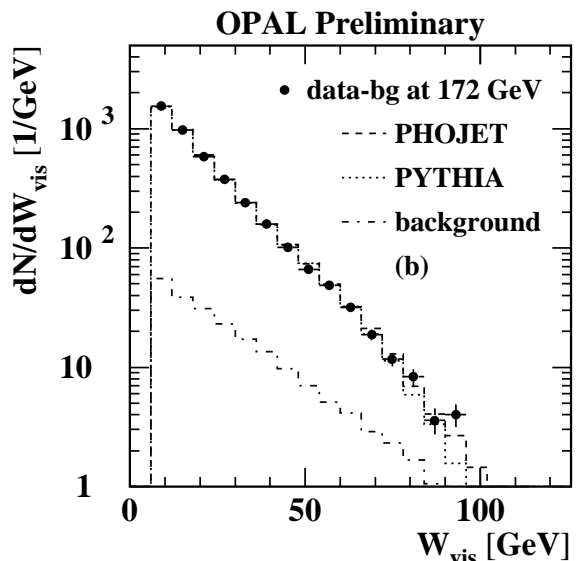

Figure 1. W_{vis} distribution for all selected events with $W_{vis} > 6$ GeV after background (bg) subtraction at $\sqrt{s}_{ee} = 172$ GeV compared to MC predictions. Statistical errors only are shown.

6. Unfolding of the hadronic cross section

The differential cross-section $\mathrm{d}\sigma_{ee}/\mathrm{d}W$ for the process $e^+e^- \to (e^+e^- + \text{hadrons})$ has to be obtained from the W_{vis} distribution. The correlation between W_{vis} and the generated invariant mass W for all selected PHOJET and PYTHIA events is shown in Fig. 2. The correlation is not very good due to hadrons which are emitted at small polar angles θ. These hadrons are either lost in the beam pipe or they are only detected with low efficiency in the electromagnetic calorimeters in the forward regions (FD and SW). The acceptance for PYTHIA is about 15% lower than for PHOJET at $W = 40$ GeV and it approaches the PHOJET acceptance of 60–65%
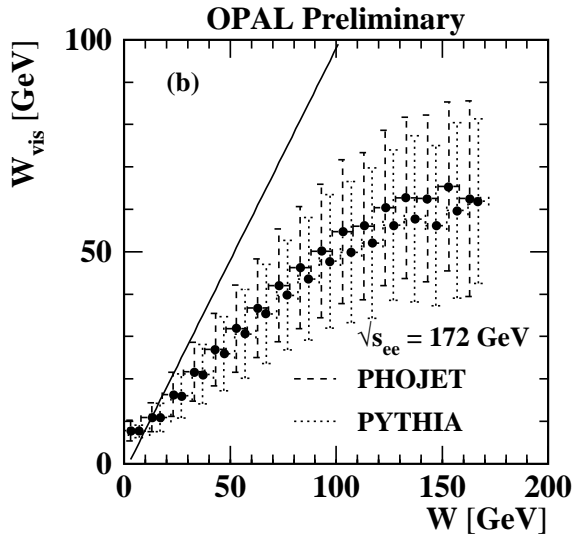
Figure 2. Correlation between W_{vis} and the generated invariant mass W at $\sqrt{s}_{ee} = 172$ GeV for MC events. The vertical bars show the standard deviation (spread) of the W_{vis} distribution in each bin. For illustration purposes the points have been shifted by ± 2 GeV.

Figure 3. The ratio of the number of selected events, N_{sel}, to the number of generated events, N_{gen}, at a given generated invariant mass W at $\sqrt{s}_{ee} = 172$ GeV for MC events. The lower curves give this ratio for the diffractive and elastic events separately.

for $W > 80$ GeV (Fig. 3). The unfolding of these resolution effects, the correction for the detector acceptance and the background subtraction is done by applying the unfolding program RUN [12]. The subtracted background does not include the remaining beam-gas and beam-wall interactions. Since the chosen bin size is not much larger than the resolution, bin-to-bin correlations are still sizeable.

The differential cross-section $d\sigma_{ee}$ of the process $e^+e^- \rightarrow (e^+e^- + \text{hadrons})$ can be translated into the cross-section $\sigma_{\gamma\gamma}$ for the process $\gamma\gamma \rightarrow \text{hadrons}$ using the luminosity function $L_{\gamma\gamma}$ for the photon flux [7],[13],[14]

$$\frac{d\sigma_{ee}}{dy_1 dQ_1^2 dy_2 dQ_2^2} = \sigma_{\gamma\gamma}(W, Q_1^2, Q_2^2) \frac{d^4 L_{\gamma\gamma}}{dy_1 dQ_1^2 dy_2 dQ_2^2},$$

where y_1 and y_2 denote the fraction of the beam energy carried by photons with $y_1 y_2 \approx W^2/s_{ee}$ (neglecting Q^2). The cross-section for real photons ($Q^2 = 0$) is derived by using appropriate form factors $F(Q^2)$ which describe the Q^2 dependence of the hadronic cross-section:
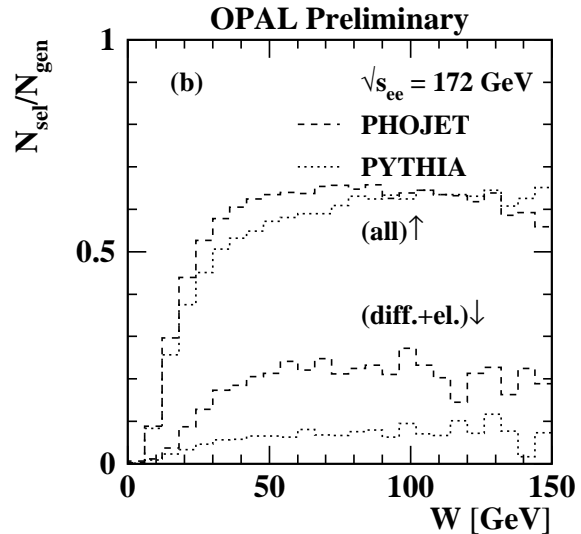
$$\sigma_{\gamma\gamma}(W, Q_1^2, Q_2^2) = F(Q_1^2) F(Q_2^2) \sigma_{\gamma\gamma}(W, 0, 0)$$

The luminosity function $L_{\gamma\gamma}$ and the form factors $F(Q^2)$ for the various W bins are obtained by applying the program PHOLUM [7]. PHOLUM takes into account both transverse and longitudinally polarized photons. The uncertainty of the extrapolation to $Q^2 = 0$ is estimated to be 5–7.5% by comparing the GVDM model with a simple ρ^0 form factor [7]. This uncertainty is not included in the systematic error of the measurement.

7. Systematic errors

The two data samples at $\sqrt{s}_{ee} = 161$ GeV and 172 GeV were independently analysed and the results for the total hadronic two-photon cross-section $\sigma_{\gamma\gamma}$ are found to be in good agreement and are therefore averaged.

Several distributions of the data are compared to the PYTHIA and PHOJET simulations af-

ter detector simulation in order to study whether the general description of the data by the MC is sufficiently good to use it for the unfolding of the cross-section. The MC distributions are all normalized to the data luminosity and the background including the $e\gamma$ events with $Q^2 > 1\,\mathrm{GeV}^2$ is subtracted from the data.

In both MC models about 20% of the cross-section is due to diffractive and elastic events (e.g. $\gamma\gamma \to \rho\rho$). This fraction is almost independent of W for $W > 10$ GeV. The selection efficiency for the diffractive and elastic events is very small and, although the rate is almost the same in both models, the selection efficiencies are very different. For a generated W of 50 GeV only about 6% of all generated diffractive and elastic events are selected in PYTHIA, whereas about 20% are selected in PHOJET (Fig. 3). Due to the small acceptance the detector correction has to rely heavily on the MC simulation for this class of events.

Significant discrepancies are found in the distribution of the charged multiplicity n_{ch} measured in the tracking chambers (Fig. 4). Both MC models significantly underestimate the fraction of low-multiplicity events with $n_{\mathrm{ch}} < 6$ and overestimate the fraction of high-multiplicity events in comparison to the data.

The energy E_{FD} measured in the forward detectors (FD) is shown in Fig. 5 for all selected events with $E_{\mathrm{FD}} > 2$ GeV. The good agreement of data and MC at large E_{FD} shows that the background from multihadronic Z^0 events and deep-inelastic $e\gamma$ events is small and that this remaining background is reasonably well described by the MC

Finally we plot the ratio $P_{\mathrm{L}}/E_{\mathrm{vis}}$ of the longitudinal momentum vector P_{L} to the visible total energy E_{vis} (Fig. 6). The ratio $P_{\mathrm{L}}/E_{\mathrm{vis}}$ is peaked around 0.9 due to the Lorentz boost of the hadronic system. Data and MC are in reasonable agreement, different from the observation in Ref. [4]. Studies of beam-gas and beam-wall events show that most of these events have $P_{\mathrm{L}}/E_{\mathrm{vis}} > 0.85$. The excess of the data over the MC seen at large $P_{\mathrm{L}}/E_{\mathrm{vis}}$ is therefore consistent with 2% remaining background from beam-gas beam-wall events.
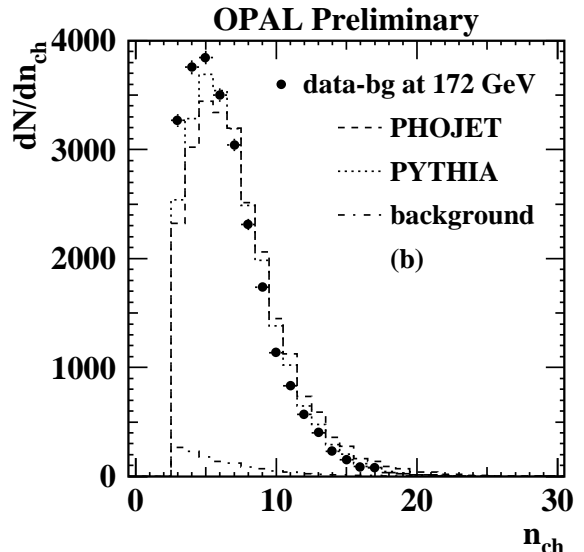

Figure 4. n_{ch} distribution for all selected events with $W_{\mathrm{vis}} > 6$ GeV after background subtraction at $\sqrt{s}_{\mathrm{ee}} = 172$ GeV compared to MC predictions. Statistical errors only are shown.

Based on these observations the following systematic errors are taken into account in the measurement of the total cross-section:

- Both MC models describe the data equally well. We therefore average the results of the unfolding. The difference between this cross-section and the results obtained by using PYTHIA and PHOJET alone are taken as systematic error.

- For data and MC the cut on the charged multiplicity n_{ch} was increased from $n_{\mathrm{ch}} \geq 3$ to $n_{\mathrm{ch}} \geq 5$. This systematically shifts the cross-sections to lower values, mainly at small W. The unfolding was also repeated using only data and MC events with $3 \leq n_{\mathrm{ch}} \leq 9$. This variation systematically increases the cross-section especially at high W where the average charged multiplicity is higher than at low W. The shifts are used as systematic errors.

- The systematic error due to the uncertainty in the energy scale of the ECAL was esti-
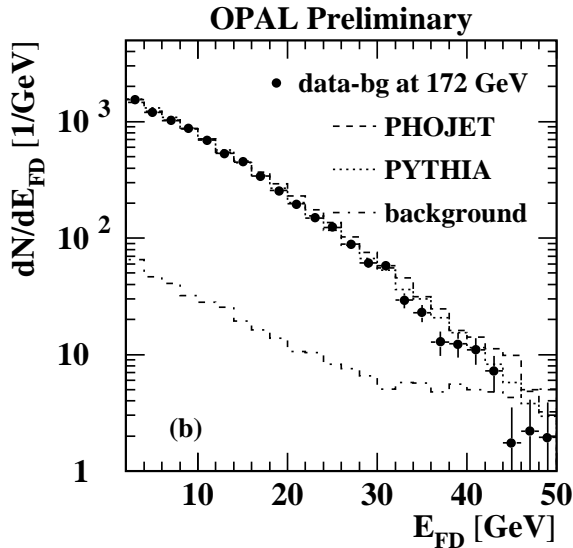
OPAL Preliminary

Figure 5. The distribution of the energy in the forward calorimeter, E_{FD}, for all selected events with $W_{vis} > 6$ GeV after background subtraction at $\sqrt{s}_{ee} = 172$ GeV compared to MC predictions. Statistical errors only are shown.
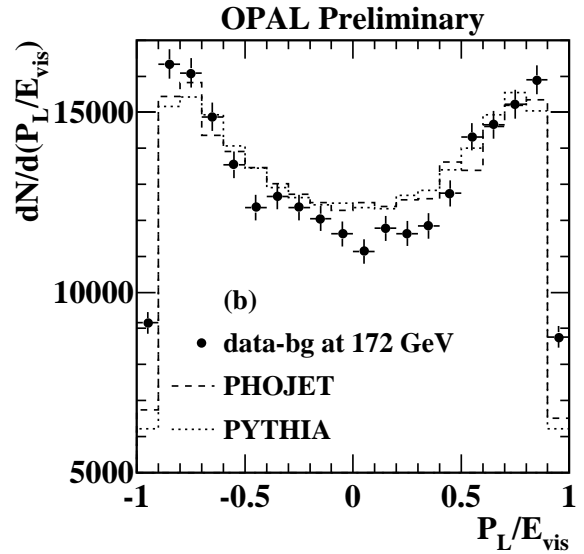
OPAL Preliminary

Figure 6. The distribution of the ratio P_L/E_{vis} for all selected events with $W_{vis} > 6$ GeV after background subtraction at $\sqrt{s}_{ee} = 172$ GeV compared to MC predictions. Statistical errors only are shown.

mated by varying the reconstructed ECAL energy in the MC by $\pm 5\%$.

- An overall normalisation uncertainty of 1% is due to the error on the luminosity measurement.

- The lower limit on the trigger efficiency is taken into account by an additional systematic error of 3% in the range $10 < W < 38$ GeV.

- It is estimated that about 2% of the selected events could be due to beam-gas or beam-wall interactions. This value is therefore taken as additional systematic error.

For the total error the statistical and the systematic errors are added in quadrature. The values are given in Table 1.

8. Results

The total hadronic cross-section $\sigma_{\gamma\gamma}$ for the process $\gamma\gamma \rightarrow$ hadrons is shown in Fig. 7. In the region $W \approx 10$ GeV the OPAL measurement is in agreement with the measurements at lower energies by PLUTO [1], TPC/2γ [2] within the experimental errors.

The OPAL measurement shows the rise in the W range $10 < W < 110$ GeV which is characteristic for hadronic cross-sections. A similar rise was observed by the L3 experiment [4], but the values for $\sigma_{\gamma\gamma}$ are about 20% lower than the OPAL measurements. Several things should be noted which can explain parts of this discrepancy: First, the errors are strongly correlated between the W bins in both experiments. Secondly, L3 has used PHOJET for the unfolding, whereas for the OPAL measurement the unfolding results of PHOJET and PYTHIA are averaged. The unfolded cross-section using PHOJET is about 5% lower than the central value. In both experiments the cross-sections obtained using PHOJET are lower than the cross-section obtained with PYTHIA.

The total cross-section $\sigma_{\gamma\gamma}$ is compared to several theoretical models. Based on the Donnachie-

W range (GeV)	10 − 16	16 − 26	26 − 38	38 − 56	56 − 80	80 −110
$\sigma_{\gamma\gamma}$ [nb]	385	394	398	433	485	536
stat.error	± 4	± 3	± 4	± 6	± 8	±15
MC model	±26	± 4	±20	±21	±21	±43
n_{ch} cut	+ 5 / − 42	+ 13 / − 37	+ 24 / − 25	+ 45 / − 21	+ 74 / − 27	+ 95 / − 34
ECAL scale	±37	±28	±13	± 6	± 6	± 7
luminosity	± 4	± 4	± 4	± 4	± 5	± 5
trigger	+12	+12	+12			
beam-gas	− 8	− 8	− 8	− 9	−10	−11
total syst.	+ 47 / − 62	+ 34 / − 48	+ 37 / − 36	+ 50 / − 32	+ 78 / − 36	+105 / − 56
total error	+ 47 / − 62	+ 34 / − 48	+ 37 / − 36	+ 50 / − 32	+ 78 / − 37	+106 / − 58

Table 1

The total hadronic two-photon cross-section $\sigma_{\gamma\gamma}$ and the contributions from the various systematic errors.

Landshoff model [15], we test the assumption of a universal high energy behaviour of $\gamma\gamma$, γp and pp cross-sections. The total cross-sections σ for hadron-hadron and γp collisions are well described by a Regge parametrisation of the form

$$\sigma = Xs^\epsilon + Ys^{-\eta}, \tag{1}$$

where $\sqrt{s}$ is the centre-of-mass energy of the hadron-hadron or γp interaction. The first term in the equation is due to Pomeron exchange and the second term is due to Reggeon exchange [16]. The factors $\epsilon = 0.0790 \pm 0.0011$ and $\eta = 0.4678 \pm 0.0059$ are assumed to be universal and have been taken from Ref. [16] together with the process dependent fit values of the parameters X and Y for the total hadronic γp and pp cross-sections. Assuming factorisation of the Pomeron term X, the total $\gamma\gamma$ cross-section can be related to the pp (or $\overline{p}$p) and γp total cross-sections at high centre-of-mass energies $\sqrt{s}_{\gamma\gamma} = \sqrt{s}_{\gamma p} = \sqrt{s}_{pp}$ where the Pomeron trajectory should dominate by

$$\sigma_{\gamma\gamma} = \frac{\sigma_{\gamma p}^2}{\sigma_{pp}}. \tag{2}$$

This simple ansatz gives a reasonable description of $\sigma_{\gamma\gamma}$. Schuler and Sjöstrand [8] give a total cross-section for the sum of all possible event classes in their model of $\gamma\gamma$ scattering where the photon has a direct, an anomalous and a VMD component. They consider the spread between this prediction and the simple factorisation ansatz

as conservative estimate of the theoretical band of uncertainty. We also plot the prediction of Engel and Ranft [7] which is implemented in PHOJET. It is in good agreement with the L3 measurement and significantly lower than the OPAL measurement. The steeper rise predicted by Engel and Ranft is in agreement with both measurements.

9. Conclusions

We have measured the total cross-section of the process $\gamma\gamma \rightarrow$ hadrons in the range $10 < W < 110$ GeV using the OPAL detector at LEP.

Both MC models used fail to describe several distributions related to the hadronic final state like the charged multiplicity distribution. Further improvements of the description of the hadronic final state are necessary to reduce the systematic error of the measurement. It will also be important to gain a better understanding of the diffractive and elastic processes for which the detection efficiency is found to be small.

With the LEP2 data the high energy behaviour of the total $\gamma\gamma$ cross-section can be studied for the first time, extending the accessible W values by one order of magnitude up to $W = 110$ GeV. We observe the rise of the total $\gamma\gamma$ cross-section characteristic for the high energy behaviour of total hadronic cross-sections. A simple model based on Regge factorisation and a universal Donnachie-Landshoff fit to the total cross-sections of γp and
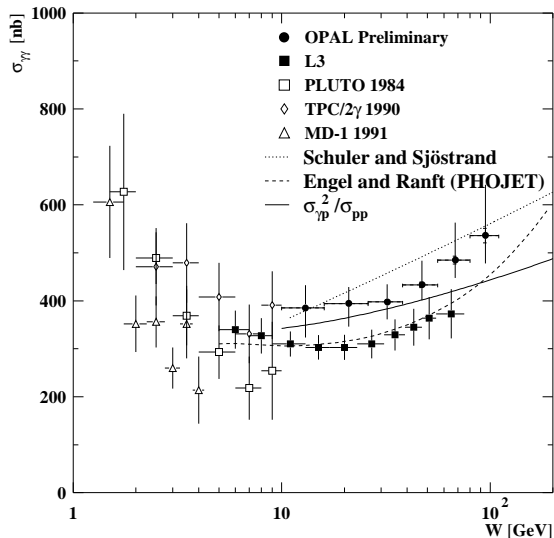
Figure 7. $\sigma_{\gamma\gamma}$ as a function of W. The OPAL measurement is compared to the measurements by PLUTO [1], TPC/2γ [2], MD1 [3] and L3 [4]. The inner error bars, which are sometimes smaller than the symbol size, give the statistical errors and the outer error bars the total errors. The data are compared to model predictions based on a Donnachie-Landshoff fit to total cross-sections [15]. The solid line gives the prediction using equation 2. The dotted line is the model of Schuler and Sjöstrand [8]. The model of Engel and Ranft [7] used in PHOJET is shown as dashed line.

pp data describes the data reasonably well.

Acknowledgements

REFERENCES

1. PLUTO Collaboration, Ch. Berger et al., Phys. Lett. B149 (1984) 421.

2. TPC/2γ Collaboration, H. Aihara et al., Phys. Rev. D41 (1990) 2667.
3. S. E. Baru et al., Z. Phys. C53 (1992) 219.
4. L3 Collaboration, M. Acciarri et al., CERN-PPE/97-48 (1997).
5. For a general review see: H. Kolanoski, *Two-Photon Physics at* e$^+$e$^-$ *Storage Rings*, Springer-Verlag (1984).
6. T. Sjöstrand, Comp. Phys. Commun. 82 (1994) 74; LUND University Report, LU-TP-95-20 (1995).
7. R. Engel and J. Ranft, Phys. Rev. D54 (1996) 4244; R. Engel, Z. Phys. C66 (1995) 203 and private communications.
8. G. A. Schuler, T. Sjöstrand, Z. Phys. C73 (1997) 677.
9. A. Capella, U. Sukhatme, C. I. Tan, J. Tran Thanh Van, Phys. Rep. 236 (1994) 225.
10. G. A. Schuler and T. Sjöstrand, Z. Phys. C68 (1995) 607.
11. M. Glück, E. Reya, A. Vogt, Phys. Rev. D46 (1992) 1973; Phys. Rev. D45 (1992) 3986.
12. V. Blobel, DESY-84-118 (1984); Proc. 1984 CERN School of Computing, Aiguablava, Spain, CERN 85-09 (1984); *The RUN manual*, unpublished.
13. V. M. Budnev et al, Phys. Rep. 15 (1975) 181-282.
14. G. A. Schuler, CERN-TH/96-297 and hep-ph/961040 (1996).
15. A. Donnachie and P. V. Landshoff, Phys. Lett. B 296 (1992) 227.
16. Review of Particle Physics, Phys. Rev. D54 (1996) 191.